THE AMERICAN SOCIETY OF MECHANICAL ENGINEERS
345 E. 47 St., New York, N.Y. 10017

92-G

Experimental Study on the Three Dimensional Flow Within a Compressor Cascade With Tip Clearance: Part II—The Tip Leakage Vortex

SHUN KANG* and CH. HIRSCH**

Vrije Universiteit Brussel, Department of Fluid Mechanics
Pleinlaan 2, 1050 Brussel, Belgium

Abstract

An analysis of the experimental data of a linear compressor cascade with tip clearance is presented with special attention to the development of the tip leakage vortex. A method for determining the tip vortex core size, centre position and vorticity or circulation from the measured data is proposed, based on the assumption of a circular tip vortex core. It is observed that the axial velocity profile passing through the tip vortex centre is wake-like. The vorticity of the tip vortex increases rapidly near the leading edge and reaches its highest values at a short distance downstream, from which it gradually decreases. In the whole evolution, its size is growing and its centre is moving away from both the suction surface and the endwall, approximately in a linear way.

Nomenclature

c	= blade chord
C_p	= static pressure coefficient
C_{pt}	= total pressure coefficient
l	= blade span
L_y	= coordinate of the tip vortex centre from low wall
L_z	= coordinate of the tip vortex centre from suction side
LE	= leading edge
PS	= pressure side
p_t	= total pressure
R	= vortex core radius
s	= pitch
SS	= suction side
TE	= trailing edge
u, v, w	= axial, spanwise and pitchwise velocities
u_t	= blade speed
V_1	= inlet resultant velocity
V_u	= circumferential velocity of a vortex
x, y, z	= axial, spanwise and pitchwise distances
β_1, β_2	= inlet and outlet flow angles
β_m	= average flow angle, midspan flow angle
Γ	= circulation
ρ	= density
τ	= tip clearance
ω	= angular velocity
$\Omega_x, \Omega_y,$	
Ω_z, Ω_s	=axial, spanwise, pitchwise and streamwise vorticities

Introduction

The study of the tip leakage vortex through the vorticity field has received an increasing interest in the published literature. Lakshminarayana and Horlock (1962) analysed the vorticity of the tip leakage vortex for an isolated compressor blade by employing a vortexmeter. The determination of vorticity directly from the measured velocity field was done recently by Inoue and Kuroumarou (1984) on the flow field behind an axial compressor rotor, and Gregory-Smith et al. (1988) in an axial turbine cascade. Measurements of the circulation in the tip leakage vortex were performed by Inoue et al. (1986) for a compressor rotor and Yaras and Sjolander (1990) for a planar turbine cascade. Their data showed the behaviour of the tip vortex downstream of the cascade exit. Obviously, it is necessary to investigate the tip vortex behaviour in its whole evolving history.

The influence of the tip gap on the blade loading and on the behaviour of the whole secondary flow field has been examined in the companion part of this paper, Part I. And a multiple tip vortex structure has been deduced, based on the flow visualizations and traverse measurements, as shown in Fig.1. The vortex structure consists of three discrete vortices, i.e., tip separation vortex, secondary vortex and tip leakage vortex. This part will present further discussions on the experiment data of the linear compressor cascade with tip clearance, but with special attention to the development of the tip leakage vortex, such as the evolution of its size, centre position and vorticity or circulation.

* Ph D. Student, Permanent address: Power Engineering Dept., Harbin Institute of Technology, Harbin 150006, P. R. China

** Professor, Member ASME

Presented at the International Gas Turbine and Aeroengine Congress and Exposition
Cologne, Germany June 1-4, 1992
This paper has been accepted for publication in the Transactions of the ASME
Discussion of it will be accepted at ASME Headquarters until September 30, 1992

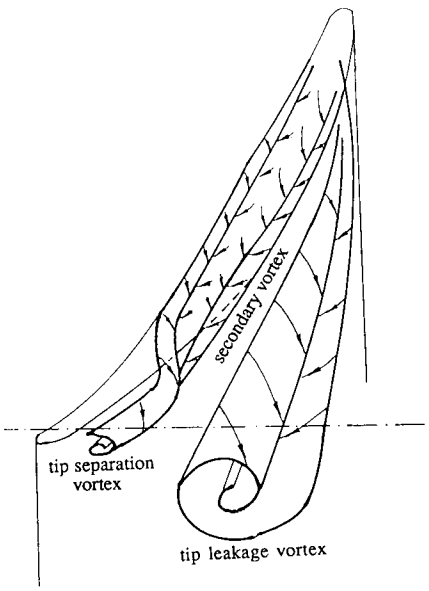

Fig.1 Schematic of the vortex structure around the tip, from Part I of this paper

Velocity Profiles

The velocity profiles near the tip leakage vortex axis are examined first. The vortex axis is defined here as the line passing through the vortex centre and is mainly along the chordwise direction.

Figure 2 shows the spanwise distribution of the axial and pitchwise velocities and the pitchwise distribution of the spanwise velocity, as an example, for 2.0% tip clearance at different axial position. It is found that the axial velocity (Fig.2a) in all the corresponding traversed planes shows a wake-like shape around the tip vortex centre. Escudier et al. (1980) reported, according to their study on the classification of confined vortex flow regimes, that at sufficiently high Reynolds number the vortex core is turbulent and its profile is wake like. In the present case, at a Reynolds number of 2.9×10^5, the inlet boundary layer flow is turbulent. Hence the core of the tip vortex, formed from the leakage flow mostly coming from the endwall and blade surface boundary layers (see Part I), should be turbulent. The growth of the depression part of the axial velocity profiles with axial distance shows the growth of the tip vortex core. It is observed that inside the passage the wake-like profile is sharp but diffuses rapidly behind the cascade. Comparing the profiles for two tip clearances, it is found that at 1.0% clearance the diffusion is stronger than at 2.0%. The reason may be that the vortex core at 1.0% clearance is much closer to the wall (see later discussions on the vortex centre location) and is more affected by the wall boundary layer.

The spanwise and pitchwise velocities in Fig.2b and 2c around the tip vortex centre show Z-shape profiles which indicate the rotation of the tip vortex. The nonzero values of spanwise velocity far away from the tip vortex centre is obviously associated with the evolution of the passage vortex.

Vorticity in the Whole Field

The vorticity in the measured field is calculated from the following formula, based on the definition of vorticity vector with the incompressible and inviscid assumptions, see Appendix Eq.(A-4),

$$\Omega_x = \left(\frac{\partial v}{\partial z} - \frac{s}{l}\frac{\partial w}{\partial y}\right)$$

$$\Omega_y = \frac{v}{u}\Omega_x + \frac{1}{2}\frac{1}{u}\frac{\partial C_{pt}}{\partial z} \qquad (1)$$

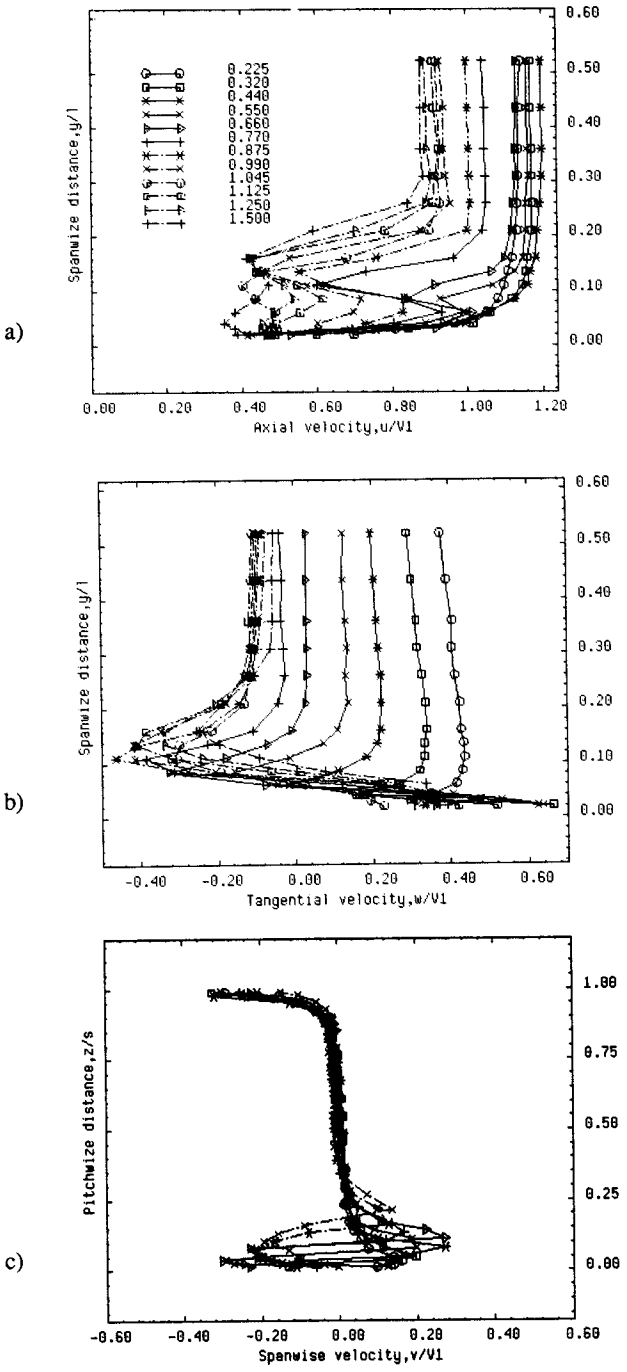

Fig.2 Profiles passing through tip vortex centre with different x/c at τ/c=0.02, a) and b) spanwise profiles of u and w, c) pitchwise profiles of v

$$\Omega_z = \frac{w}{u}\Omega_x - \frac{1}{2}\frac{1}{u}\frac{s}{l}\frac{\partial C_{pt}}{\partial y}$$

where the velocities are normalized with the inlet velocity, and y with span l, z with pitch s. A similar method was used by Gregory-Smith et. al. (1988) and Yaras and Sjolander (1990).

The illustration of vorticity signs is given in Fig.3. The isolines of the three vorticity components on the S_3 (traverse) planes are shown in

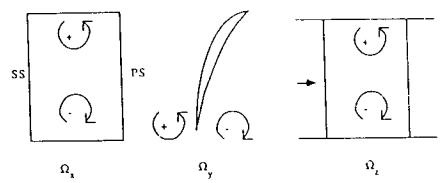

Fig.3 Illustration of vorticity signs

Fig.4, the coordinates of the traverse planes being given in Fig.1 of Part I. Figure 5 shows the vorticity vectors on the S_3 plane No.15 at the clearance of 0.0, 1.0 and 2.0%. These plots are directly drawn from the data calculated by using Eq.(1) without any smoothing. Hence the unrealistic values in some points may be due to the differentiation of the scattered experimental data.

It is seen from Fig.4b that the pitchwise vorticity across the pitch is uniform near the endwall in the S_3 plane No.1, 7.5% chord upstream of the leading edge. This shows the uniform shear flow of the inlet boundary layer. But the minus values (see Fig.3 for sign definition) of the axial vorticity (Fig.4a) near the endwall in the plane is partly due to the turning of the inlet vorticity filament, and indicates the early stage of the passage vortex. Starting from the S_3 plane No.3 (11% chord) the axial vorticity shows remarkably high values in the suction side corner. The quasi-circular isovorticity lines with positive values in the corner refers to the tip vortex core, according to the sign definition given in Fig.3, and the negative values over a large range of the passage represent the passage vortex. It is observed by using the CFView visualization program that, due to the interaction of the tip leakage vortex with the passage vortex, a relatively small region with higher negative value is formed above the tip vortex after the S_3 plane No.5 (32% chord). It can be deduced that there might be a three dimensional surface with zero vorticity, surrounding the tip vortex.

Behind the cascade exit, for example on the S_3 plane No.16 in Fig.4a, the flat elliptic loops with their long axis along the spanwise direction is refereed to the trailing vortex sheet. Because of the two dimensional geometry, comparatively little vorticity is shed in the wake and the wake is not quite clear on the streamwise vorticity plots. But from the contours of spanwise vorticity (Fig.4c), the wake can be easily identified from the straight isolines perpendicular to the endwall near midspan. Also from the vector plots in Fig.5, it is seen that the spanwise vorticity in the two sides of the wake has opposite directions, directed towards the endwall in the pressure side or towards the midspan in the suction side.

As expected, the contours of spanwise (Fig.4b) and pitchwise vorticities (Fig.4c) show two loops, with opposite sign values, in the two sides of the tip vortex centre, due to the depression of the velocity profiles in Fig.2. Because of the influence of the endwall and blade suction surface boundary layers on the tip vortex motion, the two loops are not exactly symmetric. Even so, it still can be suggested with fair confidence, based on the closed circular isolines of the total and static pressure coefficients (see Fig.9 in Part I) and the axialwise vorticities (Fig.4a) around the tip vortex centre, that after the tip vortex is rolled up, i) its core is circular; and ii) the variation of the vorticity inside its core is linear and axially symmetric. This feature of axial symmetry was also reported by Yaras and Sjolander (1990) from their downstream measurements on a turbine blade cascade.

In addition, the rolling up process of the leakage vortex can be clearly observed from the vorticity vector plots in the traverse planes, for example in the S_3 plane No.15 for 1.0% and 2.0% clearances in Fig.5. As a comparison, Figure 5 also shows the vorticity vector plots in the same plane at zero tip clearance, from which the skewed wake due to the interaction of the passage secondary flow, the concentrated shed vortex defined in the previous paper (Kang and Hirsch, 1991) and the corner vortex close to the wall can be identified.

Vorticity of the Tip Vortex Core

To explore the features of the tip vortex, based on the experimental

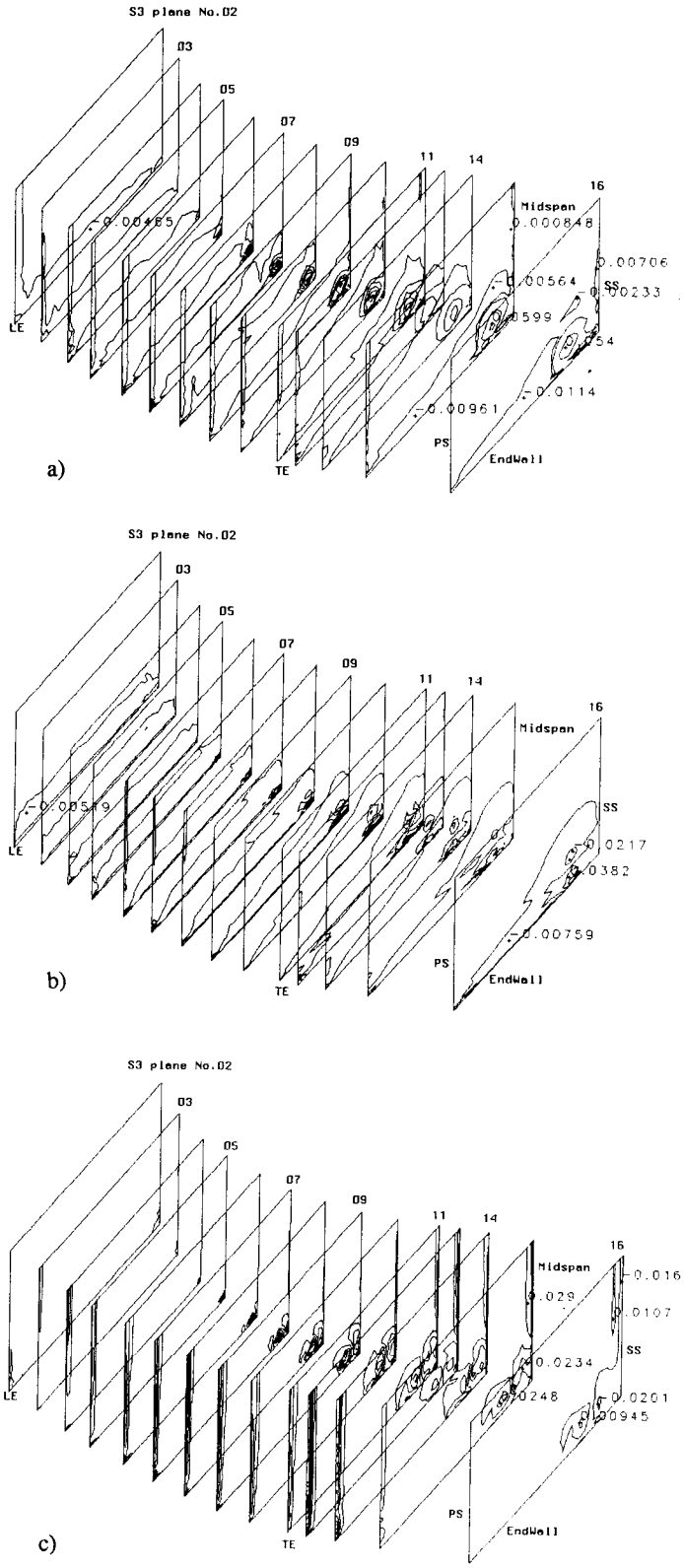

Fig.4 Contours of vorticities at τ/c=0.02, a) axial vorticity, b) pitchwise vorticity, c) spanwise vorticity

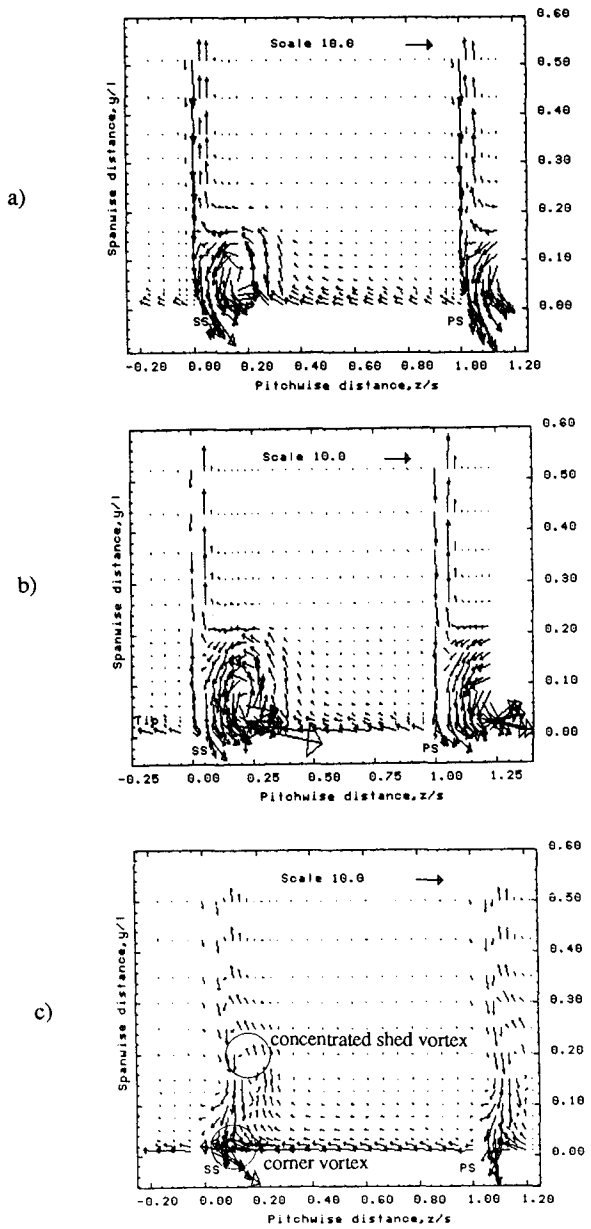

Fig.5 Vector plots of vorticity on the S_3 plane No.15 for a) $\tau/c=0.01$, b) $\tau/c=0.02$ and c) $\tau/c=0.0$

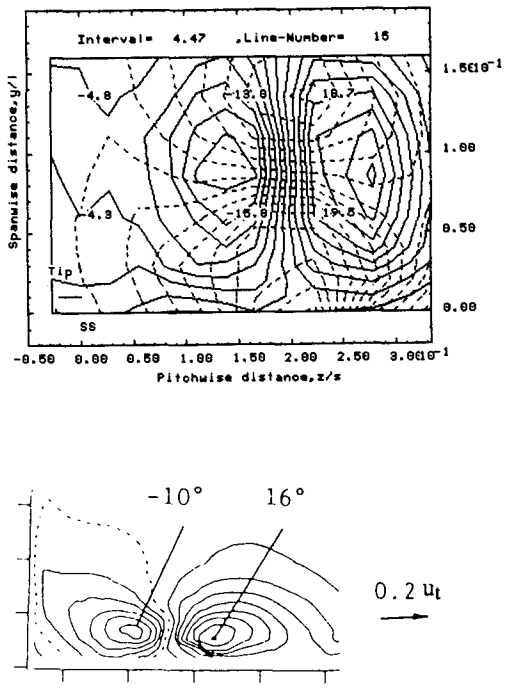

Fig.6 Isolines of flow angles; a) measured spanwise (solid lines) and pitchwise (dashed lines) flow angles in the S_3 plane No.15 at $\tau/c=0.01$, in which the numbers are the values of spanwise flow angle, and b) after Inoue et al.(1989)

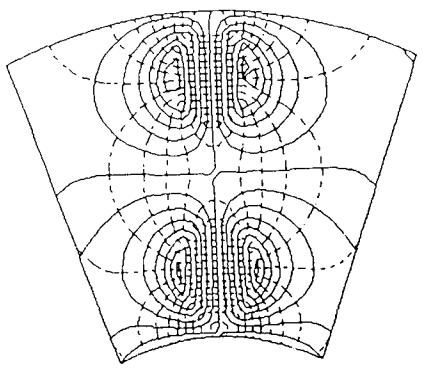

Fig.7 Isolines of spanwise (solid lines) and pitchwise (dashed lines) flow angles within an annular cascade with a pair of imaginary vortices with a circular core

data, an approximate method based on the supposition that the vortex has a circular core and its vorticities are all concentrated inside the core, is developed. The tip vortex is considered as a Rankine vortex and rotates as a solid body with constant angular velocity $\omega/2$. The size and centre location of the tip leakage vortex in each of the traverse planes can be determined from the isoline plots of the measured spanwise and pitchwise flow angles. As an example, Figure 6a shows the isolines of the measured flow angles in the S_3 plane No.15 (25% chord behind the cascade) for 1.0% clearance, As a comparison, Figure 7 shows the isolines of the flow angles induced by a pair of vortices, imagined in a passage of an annular cascade, with circular solid body cores. Two conclusions can be drawn out from these two plots: i) the vortex centre is located at the cross point of the isolines of the two flow angles with zero value; ii) the diameter of the vortex core is approximately equal to the length of the straight portion, passing through the vortex centre, along either of the flow angle contours.

With these two conclusions, the geometry of the tip leakage vortex, characterized by L_y, L_z and core radius R defined in Fig.8, can be determined from the experimental data. Consequently, its vorticity and circulation can be calculated in the following approximate way. Since the circumferential velocity V_u induced by a vortex with circular solid core takes its largest values along the edge of the solid core, it can be approximately read from the experimental data of spanwise velocity component v in the point where $y=L_y$, $z=L_z+R$. If the spanwise velocity at this point is not the largest, then, the largest in the small region around it is taken as V_u. Thus the vorticity and circulation,

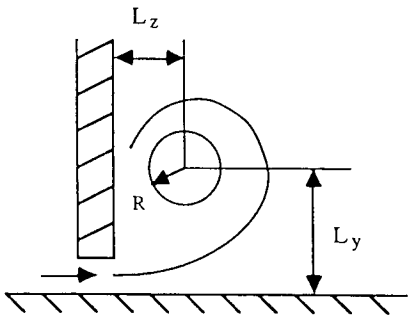

Fig.8 Definition of tip vortex geometry

normalized by V_1/s and $V_1 s$ respectively, can be calculated from following formula

$$\omega = 2\frac{V_u/V_1}{R/s} \text{ and } \Gamma = \pi\omega\frac{R^2}{s^2} \qquad (2)$$

Geometry of the Vortex Core Figure 9 shows the measured positions, L_y and L_z, of the tip vortex core centre and Figure 10 shows its core radius R for two values of tip clearance. The zero point of L_z within the passage is in the suction side, as shown if Fig.8, behind the exit it is on the line drawn from the blade trailing edge in the direction of the designed outflow angle. The values of L_z at x/c=0.0 and 0.11 in dot-and-dash lines correspond to the positions where the streamwise vorticities at the same axial coordinate take the largest value. In Part I, it is shown that a horseshoe vortex is formed in front of the blade leading edge, at the measured clearance cases, and its suction side leg is merged together with the rolling-up leakage flow in some distance downstream. Hence, the values at x/c=0.0 is most probably the centre of the suction side leg of the horseshoe vortex. It is seen that the horseshoe vortex, acted by the traverse pressure gradient, is quickly moved towards the suction side, from L_z/s=0.3 at x/c=0.0 to 0.025 at x/c=0.11 for 1.0% tip clearance as an example, and the suction side leg of the horseshoe vortex is closer to suction side at larger clearance. It is observed from Fig.9 and 10 that as the tip vortex stretches toward downstream, the centre of the tip vortex is gradually moving far away from both of the solid walls, characterized with the growth of L_y and L_z, with its core radius R growing. The growths of L_y and L_z almost obeys a linear relation with the axial distance. With increasing clearance, the spanwise coordinate of the vortex centre is increased, but the pitchwise coordinate inside the passage changes less.

Chen et al. (1991) proposed a formula to predict the pitchwise position of the tip vortex centre inside the compressor passage, based on similarity analysis, as

$$\frac{L_z/s}{x/c} = A\left(\sqrt{\frac{c\,(\tan\beta_1 - \tan\beta_2)}{s\cos\beta_m}}\right)_{\text{midspan}} \qquad (3)$$

They suggested the constant A=0.46. But it is seen from Fig.9 that for the present linear cascade with stationary endwall, the data are rather close to A=0.19.

Yanagida (1989) and Inoue and Kuroumaru (1989) measured the tip vortex trajectories from the coordinates of the low total or static pressures on the endwall. These data were used by Chen et al. (1991) to set up their model. The large difference between the model and the present data in the line slope, i.e., the constant A, may be partly related to the different way of determining the centre location, and partly to the influence of the relative motion between the blade tip and the endwall. The action of the relative motion tends to drag the tip vortex towards the pressure side in compressor cascades. It is seen from Fig.6 that the isolines of the pitchwise flow angle inside the tip

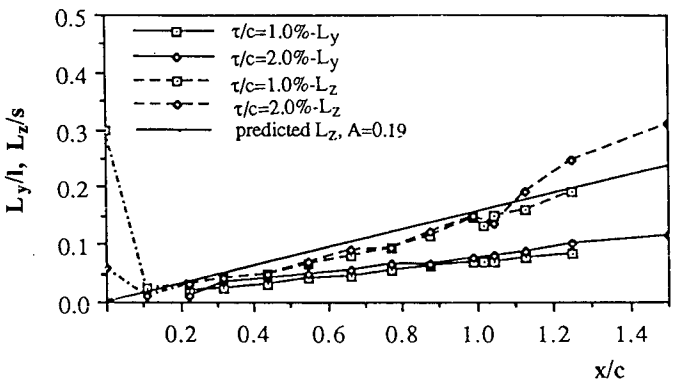

Fig.9 Evolution of tip vortex core location in the main stream direction, compared to the predications by Chen et al.(1991). The dot-dashed lines correspond to the positions of maximum streamwise vorticity

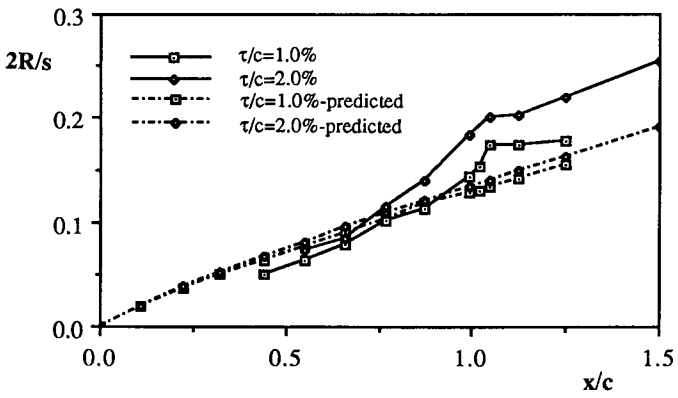

Fig.10 Evolution of the core radius in the main stream direction, with predictions following Lakshminarayana(1970)

vortex core are perpendicular to the endwall for the present stationary cascade (Fig.6a) but seriously inclined against the wall for the case (Fig.6b) of Inoue and Kuroumaru (1989). These inclined isolines will doubtlessly effect the local static and total pressure distribution on the wall. Therefore, both of the methods for determining tip vortex trajectory from the low static and/or total pressure positions on the wall are not accurate, especially when the influence of the relative motion and other kinds of secondary flows are strong.

The core radius R presented in Fig.10 is the averaged value of those measured respectively in spanwise and pitchwise directions from the isoline plots of the flow angles (Fig.6a). Because of the constraint of the present facility, the scales of the tip leakage vortex close to the leading edge plane can not be determined from the plots of flow angles. It is seen that downstream of the exit, the core radius varies in the axial direction with nearly a linear relation. The different behaviour of the core radius inside and outside the passage may be related to the different behaviour of the vortex in the two regions. Inside the passage, except for viscous diffusion, the rolling up of the vorticity near the tip dominates its behaviour. But downstream it mainly decays with distance due to fluid viscosity. The rapid increment of the radius immediately downstream of the exit may be due to the sudden release of the blade boundary.

Based on inviscid flow and constant blade loading along the chord, Rains (1954) set up a theory to predict the tip vortex radius, which has been used by Lakshminarayana (1970) in his theoretical model. Comparing the values predicted with the present data by using Rains' method, it is noted in Fig.10 that caution should be taken when using

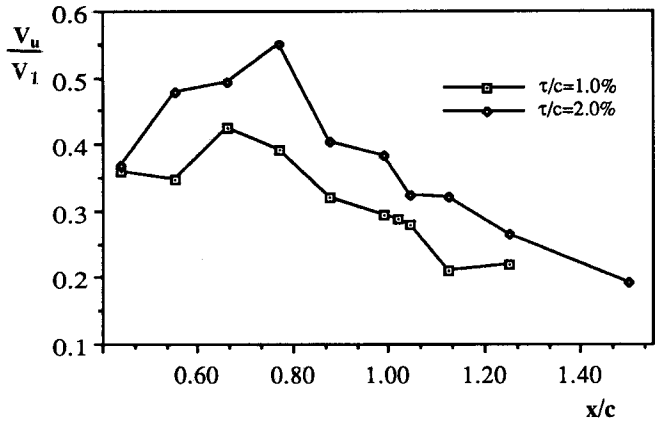

Fig.11 Evolution of the circumferential velocity at the tip vortex edge

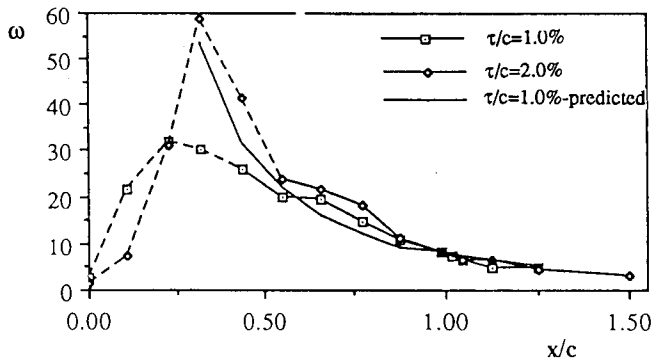

Fig.12 Evolution of the vorticities of the tip vortex core, with the predicted values following Lakshminarayana(1970)

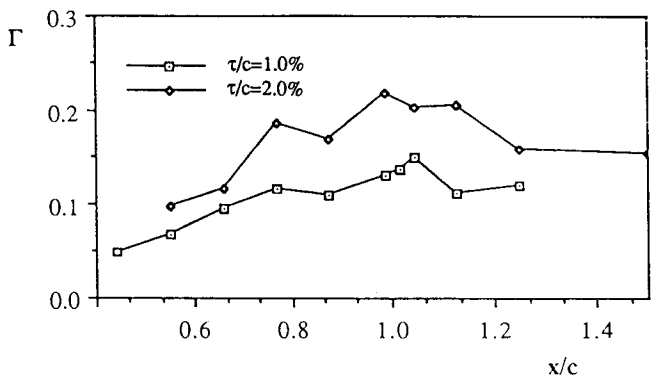

Fig.13 Evolution of the circulations of the tip vortex core

it in the rear portions and downstream of the passage. In addition, the experimental data show a stronger dependence upon the clearance level than the predictions.

Vorticity and Circulation of the Vortex Core The obtained circumferential velocities in the vortex core edge on each of the traverse planes are shown in Fig.11 for the two clearances. With the known values V_u, the vorticities (or angular velocities) and circulations can be calculated from Eq.(2) as shown in Fig.12 and 13. Due to the measurement difficulty, the information on the vorticity of the tip vortex close to the leading edge is missing. The curves drawn near the leading edge (x/c<0.44) with dashed line in Fig.12 is the largest streamwise vorticity, calculated with Eq.(A-5), in the suction side corner. This portion of the curves refers to the suction side leg of the horseshoe vortex and the early stage of the tip leakage vortex. From Fig.12, more conclusions can be drawn on the features of the tip vortex: in the leading edge plane a weak horseshoe vortex is formed with relative less vorticity, then the vorticity is increased rapidly with the leakage flow and the size of the tip vortex core is small. It achieves its largest value at a point after a short distance downstream. Even though the subsequent leakage flow still tends to increase the vorticity, the vorticity decay and streamwise adverse pressure gradient are also increased. And also the growth of the core radius reduces the vorticity, averaged over the core cross area.

Figure 12 also shows predictions according to Lakshminarayana (1970). Since the predicted vorticity is less dependent on the tip space, except near the leading edge, only the prediction on 1.0% clearance case are presented in Fig.12. It is seen that the predictions show good correlation with the experimental data in the rear part of the passage and downstream.

With the vorticity of the tip vortex monotonously decreasing in the rear part of the passage, the corresponding circulation shown in Fig.13, however, increases with a peak near the trailing edge. The growth of the circulation indicates the increment of the total vorticity of the tip vortex minus decay and diffusion in chordwise direction. Downstream of the exit, the circulation of the tip vortex goes down rapidly and then tends to remain constant toward far downstream. The large values immediately downstream of the exit may be related to the action of the blade wake. Because the rotation sense of the tip vortex is the same as that of the trailing edge vortex, some of the vorticities of the trailing vortex sheet, close to the tip vortex, are merged into the tip vortex as seen from the vector plot of Fig.5. Further downstream, its circulation is quickly decreased. It is seen that with the increasing of the tip clearance the circulation increases.

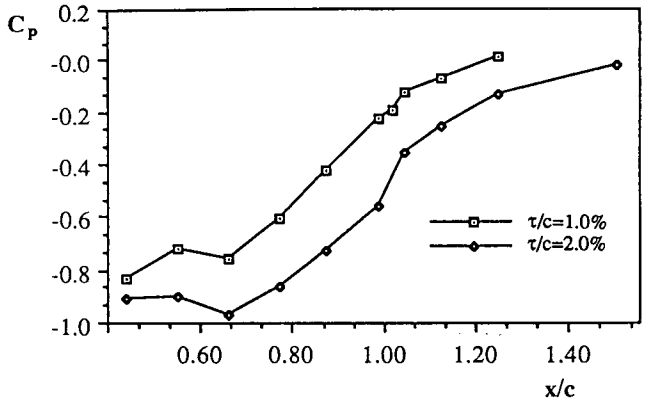

Fig.14 Static pressure at the centre of the tip vortex core

Static Pressure at the Vortex Centre Figure 14 shows the static pressure coefficients at the tip vortex centre. Normally, the static pressure is the lowest in the region within the vortex core. It is seen that the static pressure at the vortex centre is basically increasing with distance for the two tip clearances, but is decreasing with tip clearance.

Conclusions

Detailed examination and discussion on the tip vortex formed in the linear compressor cascade at design conditions have been presented,

from which following conclusions are drawn:

The axial velocity profile passing through the tip vortex centre shows a wake like shape, which is diffusing while moving downstream. The diffusion rate is affected by the wall boundary layer, especially when the vortex centre is closer to the wall at smaller clearance.

A new method for determining the tip vortex trajectory, core radius and vorticity from traverse measured data is proposed, based on the supposition that the core is circular. It is shown that the method has an acceptable accuracy.

It is found that the vorticity of the tip vortex increases rapidly near the leading edge and reaches it highest values at a short distance downstream of the leading edge, from which it gradually decreases towards the exit. With increasing clearance, the vortex circulation increases. The vorticity can be well predicted by the theory of Lakshminarayana (1970), except near the leading edge.

During the tip vortex evolution, its centre is moving away from both the blade suction surface and the endwall, approximately in a linear relation with distance. But it is observed that the slope of the linear relation for the pitchwise position of the tip vortex centre is greatly different from that predicted by Chen et al. (1991).

References

Chen, T. G., Greitzer, M. E., Tan, C. S., and Marble, F. E., 1991, "Similarity Analysis of Compressor Tip Clearance flow Structure," ASME J. of Turbomachinery, Vol.113, pp.260-271.

Escudier, M. P., Bornstein, J, Zehnder, J., and Maxworthy, T., 1980, "The Classification of Confined Vortex Flow Regimes," presented at The Winter Annual Meeting of ASME, Chicago, Illinois, Nov. 16-21, 1980, or ASME publications *Vortex Flows*, pp.15-24.

Gregory-Smith, D. G., Graves, C. P., and Walsh, J. A., 1988, "Growth of Secondary Losses and Vorticity in an Axial Turbine Cascade," ASME J. of Turbomachinery, Vol.110, pp.1-8.

Inoue, M., and Kuroumaru, M., 1984, "Three-Dimensional Structure and Decay of Vortices Behind an Axial Flow Rotation Blade Row," ASME J. of Eng. for Gas Turbines and Power, Vol.106, pp.561-569.

Inoue, M., Kuroumaru, M., and Fukuhara, M., 1986, "Behaviour of Tip Leakage Flow Behind an Axial Compressor Rotor," ASME J. of Eng. for Gas Turbines and Power, Vol.108, pp.7-14.

Inoue, M., and Kuroumaru, M., 1989, "Structure of Tip Clearance Flow in an Isolated Axial Compressor Rotor," ASME J. of Turbomachinery Vol.111, pp.250-256.

Kang, S., and Hirsch, Ch., 1991, "Three Dimensional Flows in a Linear Compressor cascade at design conditions," ASME paper No.91-GT-114.

Kang, S., and Hirsch, Ch., 1992, "Experimental Study on the Three Dimensional Flow within a Compressor Cascade with Tip Clearance: Part I -- Velocity and Pressure Fields," ASME paper, this issue.

Lakshminarayana, B., 1970, "Method of Predicting the Tip Clearance Effects in Axial Flow Turbomachinery," ASME J. of Basic Eng., Vol. 92, pp.467-480.

Lakshminarayana, B. and Horlock, J. H., 1962, "Tip-Clearance Flow and Losses for an Isolated Compressor Blade," ARC R&M 3316.

Rains, D. A., 1954, "Tip Clearance Flow in Axial Compressors and Pumps, California Institute of Technology," Mech. Eng. Laboratory, Report 5.

Sjolander, S. A., and Amrud, K. K., 1987, "Effects of Tip Clearance on Blade Loading in a Planar Cascade of Turbine Blades," ASME J. of Turbomachinery, Vol.109, pp.237-245.

Storer, J. A., and Cumpsty, N. A., 1991, "Tip Leakage Flow in Axial Compressors," ASME J. of Turbomachinery, Vol.113, pp.252-259.

Yaras, M., and Sjolander, S. A., 1990, "Development of the Tip-Leakage Flow Downstream of a Planar Cascade of Turbine Blades: Vorticity Field," ASME J. of Turbomachinery, Vol.112, pp.609-617.

Appendix

Calculation of Vorticity The components of the vorticity vector are obtained in the Cartesian coordinate system defined as x, y, and z in the axial, spanwise, and pitchwise direction

$$\begin{aligned}\Omega_x &= \frac{\partial v}{\partial z} - \frac{\partial w}{\partial y}\\ \Omega_y &= \frac{\partial w}{\partial x} - \frac{\partial u}{\partial z}\\ \Omega_z &= \frac{\partial u}{\partial y} - \frac{\partial v}{\partial x}\end{aligned} \qquad \text{(A-1)}$$

The axial component can be determined from the measured data in a traverse plane. Taking some assumptions, the spanwise and pitchwise components can also be obtained from such data. Assuming incompressible flow, neglecting viscous effects, the following equation can be used as an alternative way

$$\vec{V} \times \vec{\Omega} = \frac{1}{\rho} \nabla p_t \qquad \text{(A-2)}$$

Taking its y and z components,

$$\begin{aligned} w\Omega_x - u\Omega_z &= \frac{1}{\rho}\frac{\partial p_t}{\partial y}\\ u\Omega_y - v\Omega_x &= \frac{1}{\rho}\frac{\partial p_t}{\partial z}\end{aligned} \qquad \text{(A-3)}$$

If the vorticity components are normalized with inlet velocity V_1 and pitch s, for example, $\Omega_x s/V_1$, then the final formula is

$$\begin{aligned}\Omega_x &= \left(\frac{\partial v}{\partial z} - \frac{s}{l}\frac{\partial w}{\partial y}\right)\\ \Omega_y &= \frac{v}{u}\Omega_x + \frac{1}{2}\frac{1}{u}\frac{\partial C_{pt}}{\partial z}\\ \Omega_z &= \frac{w}{u}\Omega_x - \frac{1}{2}\frac{1}{u}\frac{s}{l}\frac{\partial C_{pt}}{\partial y}\end{aligned} \qquad \text{(A-4)}$$

where the velocities are normalized with inlet velocity V_1, and y with span l, z with pitch s.

The streamwise vorticity was taken as the component of vorticity in the main flow direction, defined as the midspan flow, rather than the component in the local flow direction. Thus the streamwise vorticity becomes

$$\Omega_s = \Omega_x \cos\beta_m + \Omega_z \sin\beta_m \qquad \text{(A-5)}$$

where β_m is the pitchwise flow angle at midspan but varying with pitchwise distance.